Nonlinear magnetization processes in the Landau-Ginzburg model of magnetic inhomogeneities for uniaxial ferromagnets

P. Winternitz
Centre de Recherches Mathématiques, Université de Montréal, Case Postale 6128, Succursale A, Montréal, Québec, Canada H3C 3J7

A. M. Grundland
Departément de Mathématiques et d'Informatique, Université du Québec à Trois Rivières, Trois Rivières, Québec, Canada G9A 5S7

J. A. Tuszyński
Department of Physics, University of Alberta, Edmonton, Alberta, Canada T6G 2J1
(Received 14 February 1991; revised manuscript received 27 June 1991)

In this paper we apply the Landau-Ginzburg model to a uniaxial ferromagnet including the possibility of magnetic inhomogeneities in the sample. The effects of external magnetic fields on the various homogeneous and inhomogeneous magnetic structures that minimize the free energy are studied. Using exact methods of nonlinear analysis, space-dependent solutions of the equation of state are found, and their mean magnetizations are calculated. A combination of analytical and numerical methods is then employed in the study of their energies. Finally, the role of various magnetization patterns is investigated in the Arrott plots for magnetization processes.

I. INTRODUCTION

The free-energy density f for uniaxial ferromagnets close to their critical temperature T_c can be usually written in the Landau-Ginzburg form

$$f = f_0 + \tfrac{1}{2}AM^2 + \tfrac{1}{4}BM^4 + D|\nabla M|^2 , \tag{1.1}$$

where M is the relative magnetization with respect to the saturation magnetization, measured along the easy magnetization axis. The coefficient A is typically assumed to vary linearly with reduced temperature as $A = a(T - T_c)$ while B and D are virtually constant in the neighborhood of T_c. It is also expected here that the anisotropy of the magnet in this regime is so strong that reorientation processes of the easy magnetization axis are excluded and consequently the remaining components of the magnetization vector need not be explicitly included in the model. Equation (1.1) is either postulated in a phenomenological Landau-Ginzburg model[1,2] or derived from microscopic considerations[3,4] for spin-lattice models which cover both short- and long-range interactions, and where transition to continuum limit is warranted. The addition of the Ginzburg term $D|\nabla M|^2$ reflects the presence of inhomogeneities in the system which may be of special importance in ferromagnetic materials, and in particular in dilute and amorphous alloys.[5,6] The physical origin of this term may also be found in the nearest-neighbor interactions[7] so that $D > 0$ corresponds to ferromagnetic while $D < 0$ to antiferromagnetic interactions.

In a recent paper[4] the inhomogeneous equation of state for the order parameter $M(\mathbf{x})$ was derived minimizing the free-energy functional

$$F = \int f(M, \nabla M) d^3x . \tag{1.2}$$

Using the method of symmetry reduction[8] this nonlinear partial differential equation (PDE)

$$\nabla^2 M = \frac{A}{2D} M + \frac{B}{2D} M^3 \tag{1.3}$$

was reduced to a number of ordinary differential equations (ODE's) corresponding to different boundary and initial conditions. In Eq. (1.3) ∇^2 denotes the three-dimensional Laplacian operator. Subsequently, numerous exact solutions to Eq. (1.3) were found together with the energies required for their formation.

In the present paper we extend the results of the previous study[4] to a different physical situation, namely one in which an external magnetic field H applied along the easy magnetization axis interacts with the magnetization order parameter M via the Zeeman term $-MH$. Thus, the free-energy density is now given by

$$f_H = f - MH \tag{1.4}$$

with f as in (1.1). The steady-state equation of state is found by minimizing the functional F corresponding to (1.4) and is

$$\nabla^2 M = -\frac{H}{2D} + \frac{A}{2D} M + \frac{B}{2D} M^3 , \tag{1.5}$$

where $D \neq 0$ and $B \neq 0$. The field H may take both positive and negative values depending on whether it is parallel or antiparallel to M, respectively.

Equation (1.5) for $H \neq 0$ and $B \neq 0$ is invariant only under the Euclidean group $E(3)$ of three-dimensional real

Euclidean space (x_1,x_2,x_3). The Lie algebra of this group has a basis consisting of three translations $P_i \equiv \partial_{x_i}$ and three rotations $L_i \equiv -\epsilon_{ijk} x_j \partial_{x_k}$, where ϵ_{ijk} is the Levi-Civita symbol. There are precisely three subgroups, providing reductions to ODE's. They are generated by $\{L_3,P_1,P_2\}$, $\{L_3,P_3\}$, and $\{L_1,L_2,L_3\}$ and lead to the equation

$$\frac{d^2M}{d\xi^2}+\frac{k}{\xi}\frac{dM}{d\xi}=\frac{B}{2D}\left[M^3+\frac{A}{B}M-\frac{H}{B}\right] \tag{1.6}$$

with $k=0,1,2$, respectively. Here, $M=M(\xi)$ and ξ is a so-called symmetry variable which may take one of the following three forms:

$$\xi_0=x_3,\ \xi_1=(x_1^2+x_2^2)^{1/2},\ \text{or}\ \xi_2=(x_1^2+x_2^2+x_3^2)^{1/2}\ , \tag{1.7}$$

corresponding to $k=0$, 1, and 2, respectively.

Our intention in this paper is to analyze as completely as possible the case of translationally invariant solutions, i.e., $k=0$ corresponding to the case of a long sample, for which the magnetization varies negligibly. The two remaining symmetry choices, cylindrical and spherical, are much more complicated and will be investigated separately in the future. In Sec. II we obtain the general solutions of Eq. (1.6) for $k=0$ for all possible types of initial conditions that can be imposed on a (boundary) plane. Particular attention is paid to the dependence of these solutions on the field H. Then, in Sec. III we calculate the mean magnetizations of these solutions. Sec. IV is concerned with the energies of solutions and here we employ a combination of analytical and numerical methods of calculation. Finally, in Sec. V we focus on the form of Arrott plots produced by each of the solutions in order to elucidate the question of the experimentally observed[9] curvature.

II. TRANSLATIONALLY INVARIANT SOLUTIONS

Imposing boundary conditions for Eq. (1.5) on a plane leads to solutions given by $M(\xi)$ where $\xi=\mathbf{e}\cdot(\mathbf{x}-\mathbf{x}_0)$; $|\mathbf{e}|^2=1$ so that $\mathbf{e}$ is a unit vector normal to the boundary plane. The ODE satisfied by M is Eq. (1.6) with $k=0$. This equation, for $(dM/d\xi)\neq 0$, can be integrated once to the form

$$\begin{aligned}\left[\frac{dM}{d\xi}\right]^2&=\frac{B}{4D}\left[M^4+2\frac{A}{B}M^2-\frac{4H}{B}M+C\right]\\&=\Delta(M-M_1)(M-M_2)(M-M_3)(M-M_4)\\&=R(M)\ ,\end{aligned} \tag{2.1}$$

where C is an integration constant, $\Delta\equiv B/4D$, and M_1, M_2, M_3, and M_4 are the four roots of the quartic polynomial on the right-hand side of the equation above. They depend on A, B, C, and H in an obvious way. Depending on the values of the four roots M_1, M_2, M_3, and M_4 and the sign of Δ we find different functional forms of the solutions $M(\xi)$. Our main aim in this section is to establish how the magnetic field H influences the solutions of the equation of state obtained in our earlier publication[4] when $H=0$. The assumption inherent in Eq. (1.4) is that the magnetic field is relatively weak. We can thus assume that when the magnetic field is switched off ($H\to 0$), the coefficients A, B, C, and D in Eq. (2.1) are not drastically affected, in particular, that $\Delta\equiv B/4D$ does not change its sign.

The procedure adopted here will be to integrate Eq. (2.1) explicitly and exactly for $H\neq 0$ in a manner compatible with the $H\to 0$ limit. We subsequently take this limit and then compare with the results found earlier[4] for $H=0$. In the following we shall restrict ourselves to a study of *real nonsingular* solutions. To illustrate the origin of the various types of solutions, in Fig. 1 we present the diagrams of $\dot{M}^2$ as a function of M, corresponding to Eq. (2.1) for $H\neq 0$ which cover all possible relations between the roots of the polynomial $R(M)$. Multiple roots are marked by open circles on the M axis. Real nonsingular solutions correspond to the solid curve sections, complex solutions to dotted sections, and singular solutions to dashed sections. Isolated circles (not connected by solid lines) correspond to constant solutions [see Figs. 1(c) and 1(h)]. Circles connected to solid lines are asymp-

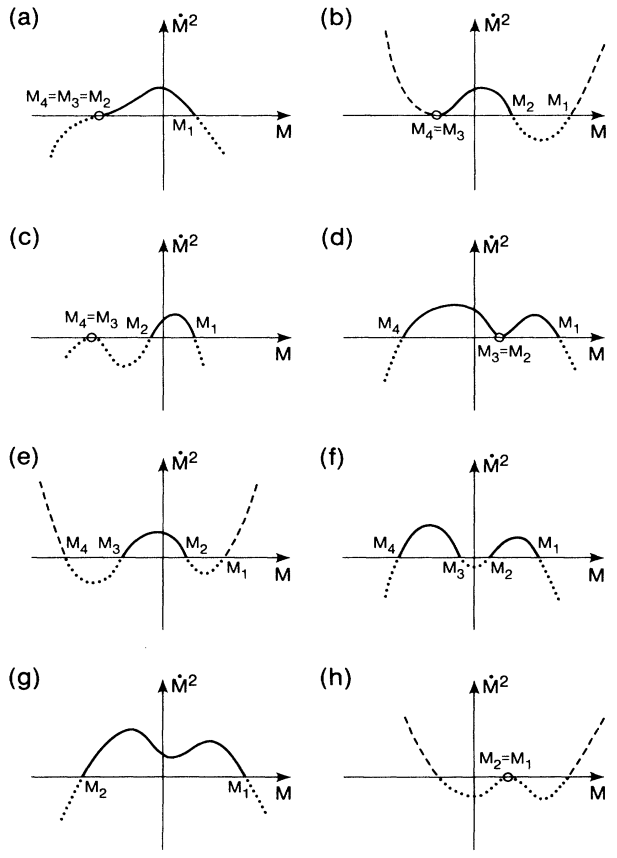

FIG. 1. The diagrams of $\dot{M}^2$ as a function of M, corresponding to real finite solutions in the presence of a magnetic field H. The dashed parts of the curves correspond to singular solutions, the dotted ones to complex ones. Each diagram has its complement in the form of the mirror image in the $M=0$ axis.

totic values of nonconstant solutions (for $\xi \to \pm\infty$). Thus, solid line sections connecting two circles are kinks (which occur for $H \to 0$), those connecting a circle and a simple root are solitary waves (bumps or wells). Solid lines connecting two simple roots correspond to periodic solutions. If the diagram has no circles (no multiple roots) solutions are obtained in terms of Jacobi elliptic functions, otherwise in terms of elementary functions. To save space we drop the diagrams that are mirror images in the $\dot{M}^2$ axis of curves that are presented. Below, each situation described by a diagram in Fig. 1 is discussed and exact formulas for $M(\xi)$ are provided.

(i) *One triple root.* $\Delta < 0$, $M_2 = M_3 = M_4 < M < M_1$, and $M_1 = -3M_2$; M_i $(1 \le i \le 4)$ are real [see Fig. 1(a)], or $M_1 < M < M_2 = M_3 = M_4$. The solution here is

$$M = M_2 \left[1 - \frac{4}{1 - 4\Delta M_2^2 \xi^2} \right] , \tag{2.2}$$

and it has the form of an algebraic solitary wave satisfying $M \to M_2$ as $\xi \to \pm\infty$ and $M = M_1$ for $\xi = 0$. This is a bump for $M_1 > 0$ and a well for $M_1 < 0$. In the limit $H \to 0$, we have $M_2 \to 0$ and $M_1 \to 0$, hence also $C \to 0$ and $A \to 0$. Thus, $M \to 0$ as $H \to 0$ is the only possible limit and this solution approaches the disordered phase. For $H \neq 0$, Eq. (2.2) describes a nucleation center of magnetic order.

(ii) *One double root, two single ones.*

(a) $M_4 = M_3 \le M \le M_2 \le M_1$, $\Delta > 0$ [Fig. 1(b)]. The real finite solution in this case has the form

$$M = M_3 + \frac{4(M_2 - M_3)E^2}{[E^2 + (m+1)^2][E^2 + (m-1)^2]} , \tag{2.3}$$

where we have denoted

$$m^2 = (M_2 - M_3)/(M_1 - M_3) ;$$

$$E = 2 \exp \left[\frac{\epsilon}{2} [\Delta (M_1 - M_3)(M_2 - M_3)]^{1/2} \xi \right]$$

with $\epsilon = \pm 1$. This describes a "bump" for Fig. 1(b) while for its mirror image in the $\dot{M}^2$ axis, the formula is the same but M represents a "well." As $\xi \to \pm\infty$, $M \to M_3$ while for $\xi = 0$, $M = M_2$. Interestingly enough, in the limit $H \to 0$, $M_2 \to M_1$ and $M_3 \to -M_1$, so that the solitary wave of Eq. (2.3) becomes the kink found in the previous paper,[4] i.e., $-\epsilon M_1 \tanh(\sqrt{\Delta} M_1 \xi)$. If, on the other hand, in the limiting procedure we also have $A \to 0$ and $C \to 0$, then $M_1 \to 0$ and the disordered phase solution $M = 0$ is approached. We conclude that Eq. (2.3) again represents a nucleation center of magnetic order.

(b) $M_4 = M_3 < M_2 \le M \le M_1$ and $\Delta < 0$ [Fig. 1(c)]. The real finite solution in this case can be written as

$$M = M_3 + \frac{2(M_1 - M_3)(M_2 - M_3)}{M_1 + M_2 - 2M_3 + (M_1 - M_2)\cos[-\Delta (M_1 - M_3)(M_2 - M_3)]^{1/2} \xi} . \tag{2.4}$$

Thus, for $H \neq 0$ M oscillates between M_2 and M_3. In the limit $H \to 0$, $M_2 \to M_1$ and the magnetization profile approaches zero, i.e., $M \to 0$ as $H \to 0$, where in general we have $M_1 \neq 0$. In conclusion, Eq. (2.4) represents either ferromagnetic or antiferromagnetic spin waves depending on whether the signs of M_1 and M_2 are the same or different.

(c) $M_4 < M_3 = M_2 \le M \le M_1$ and $\Delta < 0$ or $M_4 \le M < M_3 = M_2 < M_1$ [Fig. 1(d)]. The solution here is a solitary wave that can be written as

$$M = M_2 + \frac{(M_1 - M_2)(M_2 - M_4)}{2M_2 + \epsilon(M_1 + M_2)\cosh[-\Delta (M_1 - M_2)(M_2 - M_4)]^{1/2} \xi} , \tag{2.5}$$

where $\epsilon = \pm 1$. For $\epsilon = +1$ Eq. (2.5) describes a bump such that $M \to M_2$ as $\xi \to \pm\infty$ and $M = M_1 > M_2$ for $\xi = 0$. For $\epsilon = -1$, on the other hand, Eq. (2.5) describes a well with $M \to M_2$ as $\xi \to \pm\infty$ and $M = M_4 < M_2$ for $\xi = 0$. For $H \to 0$ we have $M_2 \to 0$, and $M_4 \to -M_1$ resulting in a pair of symmetric solitary waves: $M \to \epsilon M_1 \operatorname{sech}(\sqrt{-\Delta} M_1 \xi)$, exactly in the form found earlier.[4] Thus, it is concluded that Eq. (2.5) again represents a nucleation center.

(iii) *Four distinct real roots.* In this case solutions will always be periodic and may be physically interpreted as one-dimensional classical analogs of ferromagnetic or antiferromagnetic spin waves. There are several distinct possibilities within this category which are discussed below.

(a) $M_4 < M_3 \le M \le M_2 < M_1$, $\Delta > 0$, M_i $(1 \le i \le 4)$ are real [Fig. 1(e)]. In order to be able to take the limit of $H \to 0$ in an appropriate manner, we integrate Eq. (2.1) directly applying a fractional linear transformation

$$W = \frac{\alpha M + \beta}{\gamma M + \delta} , \tag{2.6}$$

and choose the constant coefficients $\alpha, \beta, \gamma, \delta$ conveniently, so that $M = (M_4, M_3, M_2, M_1)$ goes into $W = (-R, -1, 1, R)$, respectively, with $R > 1$. This yields

$$\begin{aligned} \alpha &= (2M_1 - M_2 - M_3)R - (M_2 - M_3) , \\ \beta &= M_1(M_2 - M_3) + [2M_2 M_3 - M_1(M_2 + M_3)]R , \\ \gamma &= 2M_1 - M_2 - M_3 - (M_2 - M_3)R , \\ \delta &= M_1(M_2 - M_3)R + 2M_2 M_3 - M_1(M_2 + M_3) , \end{aligned} \tag{2.7}$$

while the parameter R is found to be

$$R=[(M_1-M_4)(M_2-M_3)]^{-1}\times\{-2M_1M_4-2M_2M_3+(M_1+M_4)(M_2+M_3)+2[(M_1-M_2)(M_1-M_3)(M_2-M_4)\times(M_3-M_4)]^{1/2}\}\ . \tag{2.8}$$

As a result, Eq. (2.1) reduces to a standard equation for a Jacobi elliptic function[10] and we obtain two different types of solutions. First,

$$M(\xi)=\frac{\delta\,\mathrm{sn}(\sqrt{\Delta K_0}R\xi,k)-\beta}{\alpha-\gamma\,\mathrm{sn}(\sqrt{\Delta K_0}R\xi,k)}\ , \tag{2.9}$$

where $k=R^{-1}$ is the Jacobi modulus and

$$K_0\equiv[(M_1-M_4)(M_2-M_3)(R-1)-2(M_1-M_2)(M_3-M_4)]/2(R^2-1)>0\ . \tag{2.10}$$

In the limit $H\to 0$, (2.9) becomes one of the solutions found previously in the absence of external fields,[4] namely $M_2\,\mathrm{sn}(\sqrt{\Delta}M_1\xi,M_2/M_1)$. However, if in the limit we also have $M_2\to 0$, then $M\to 0$. If, on the other hand, we have $M_2\to M_1$ for $H\to 0$, then a tanh kink is found.

(b) $M_4\le M\le M_3<M_2<M_1$ and $\Delta<0$, or $M_4<M_3<M_2\le M\le M_1$ and $\Delta<0$ [Fig. 1(f)]. This solution is given by

$$M=\frac{\epsilon\delta R\,\mathrm{dn}(\sqrt{-\Delta K_0}R\xi,k)-\beta}{\alpha-\epsilon\gamma R\,\mathrm{dn}(\sqrt{-\Delta K_0}R\xi,k)}\ , \tag{2.11}$$

where $k=\sqrt{1-R^{-2}}$, $\epsilon=\pm 1$, and α, β, γ, δ, are those of Eq. (2.7), R is in Eq. (2.8), and K_0 in Eq. (2.10). As $H\to 0$, $M\to\epsilon M_1\,\mathrm{dn}(M_1\sqrt{-\Delta}\xi,k)$ with $k=(1-M_2^2/M_1^2)^{1/2}$, in perfect agreement with one of the solutions found earlier.[4] If $M_2\to 0$ in addition to $H\to 0$, we obtain the sech-solitary waves. If $M_2\to M_1$ we obtain the constant solutions $M\to\epsilon M_1$, and for $M_2\to 0$ and $M_1\to 0$ the disordered phase results since $M\to 0$.

(iv) *Two distinct real roots and two complex conjugate ones.* We put $M_2<M_1, M_{3,4}=p\pm iq$ where $q>0$, $\Delta<0$ [Fig. 1(g)]. In this case the solution can be found directly[10] as

$$M=\frac{(M_2A-M_1B)\mathrm{cn}(\sqrt{-\Delta AB}\,\xi,k)+M_2A+M_1B}{(A-B)\mathrm{cn}(\sqrt{-\Delta AB}\,\xi,k)+A+B}\ , \tag{2.12}$$

where $A^2\equiv(M_1-p)^2+q^2$; $B^2=(M_2-p)^2+q^2$, and $k^2=[(M_1-M_2)^2-(A-B)^2]/4AB$. When $H\to 0$, then $M_2\to -M_1$ and $p\to 0$ which yields $M\to -M_1\mathrm{cn}([-\Delta(M_1^2+q^2)]^{1/2}\xi,k)$, where $k=M_1/(M_1^2+q^2)^{1/2}$, in agreement with our earlier calculations.[4] We may also have $q\to 0$ as $H\to 0$, whereupon $M(\xi)$ tends to the sech-solitary wave solution. Alternatively, if $M_1\to 0$ as $H\to 0$, then M becomes the disordered phase solution, $M\to 0$.

(v) *Constant solutions.* In addition to the inhomogeneous solutions of (i)–(iv), constant (mean field) solutions of the equation of motion are directly found which satisfy the homogeneous equation of state[11]

$$H=AM+BM^3\ . \tag{2.13}$$

Note that they have been represented in Figs. 1(c) and 1(h) using the isolated circles. For $H\to 0$ we obviously have $M\to 0$ or $M\to\pm\sqrt{-A/B}$. With $A=a(T-T_c)$ the magnetization M is a single-valued function of H for $T>T_c$. For $T<T_c$ and $-(-A/B)^{1/2}<M<(-A/B)^{1/2}$, M as a function of the field H exhibits a typically hysteretic behavior. The constant values of M correspond to multiple roots on the plot of M^2 versus M. In particular $M=0$ is a quadruple root; $M=\pm(-A/B)^{1/2}$ for $(-A/B)>0$ are two double roots.

We close this section by providing a physical interpretation of the obtained solutions. First, the constant solutions correspond to equilibrium (when $A+3BM^2\ge 0$) or unstable (otherwise) mean field or homogeneous phases in the system. The nonsingular elementary solutions (algebraic or hyperbolic) represent two classes of localized order parameter structures. They describe either nucleation centers of magnetic order (algebraic or sech type) or domain walls separating energetically equivalent phases (kinks). Nonsingular periodic solutions are expressed either through trigonometric or elliptic functions. Depending on their type and specifically whether or not they oscillate crossing the $M=0$ point, they can be interpreted as classical analogs of either ferromagnetic (if they do not) or antiferromagnetic (if they do) spin waves. The analogy here is, of course, not complete since ferromagnetic or antiferromagnetic spin waves are usually transverse, dynamical oscillations. The model presented here is static (no time dependence) and the solutions are necessarily longitudinal since the order parameter is one component. We have reason to believe, however, that similar patterns also exist in time-dependent extensions of the presented model as well as in two-component ones where the magnetization represents a rotating vector.

III. MEAN MAGNETIZATION

In Sec. II we have obtained a complete list of all nonsingular real translationally invariant solutions of the static Landau-Ginzburg equation (1.5) for arbitrary external magnetic fields H. We thus have explicit expressions of the magnetization profiles $M(\xi,H)$ as a function of the spatial coordinate $\xi=(\mathbf{e},\mathbf{x}-\mathbf{x}_0)$ and parametrized by the magnetic field H. The obtained solutions were found to be constant, localized, or periodic in space. For $H\neq 0$ the localized ones are always in the form of solitary waves (bumps or wells). When the field is switched off ($H\to 0$) the solitary waves either vanish, go over into

kinks, or remain as solitary waves. Periodic waves may either vanish when $H \to 0$ or remain periodic and degenerate special cases may also occur.

In experimental studies, the measured quantity is a mean magnetization $M(H)$ averaged over the length of the sample. To establish a direct connection with experiment, in this section we shall calculate exactly mean magnetizations corresponding to each of the exact solutions found in Sec. II. For a solution $M(\xi)$ its mean magnetization is defined through

$$\overline{M}(H) \equiv \frac{1}{L} \int_{\xi_1}^{\xi_2} M(\xi) d\xi \ , \tag{3.1}$$

where $L = \xi_2 - \xi_1$ is the characteristic length. For periodic solutions we identify L with the wavelength.

For localized solutions two different types of averages will be defined, namely $\overline{M}_\infty(H)$ corresponding to the average over the entire macroscopic sample ($L \to \infty$) and $\overline{M}_0(H)$ calculated for L taken to be the "half-width" of the solitary wave. In this latter case the limits of integration ξ_1 and ξ_2 are determined from the condition

$$M_0 \equiv \tfrac{1}{2}(M_E + M_\infty) = M(\xi_1) = M(\xi_2) \ , \tag{3.2}$$

where $M_E \equiv M(\xi_0)$ is the maximum value of $M(\xi)$ for a bump and the minimum value for a well and $M_\infty \equiv \lim_{\xi \to \pm\infty} M(\xi)$. In principle, both $\overline{M}_\infty(H)$ and $\overline{M}_0(H)$ should be observable through a measurement of scattering intensity (using, for example, neutrons) and would have to involve a very detailed scanning of the sample. Throughout this section we shall assume that $D > 0$ in Eqs (1.5) and (2.1). In each case considered the limit $H \to 0$ will be taken.

A. Localized solutions

The localized solutions can all be written as $M(\xi) = M_\infty + S(\xi)$, and we always have $\overline{M}_\infty(H) = M_\infty$, since the integral over $S(\xi)$ converges.

1. Solution (2.2) of Fig. 1(a)

For an arbitrary choice of ξ_2 we find

$$\overline{M} = M_2 + 2 \arctan[(-2)\sqrt{-\Delta} M_2 \xi_2] / \xi_2 \sqrt{-\Delta} \ , \tag{3.3}$$

where $M_2 = (-H/2B)^{1/3}$ and hence

$$\overline{M}_\infty(H) = M_2 < 0, \quad \overline{M}_0(H) = (-M_2)(\pi - 1) > 0 \ . \tag{3.4}$$

When $H \to 0$, $M_2 \to 0$ and $M(\xi) = 0$, i.e., the solution (2.2) approaches the disordered phase: $\overline{M}_\infty(0) = \overline{M}_0(0) = 0$.

2. Solution (2.3) of Fig. 1(b)

Performing the required integration we obtain

$$\overline{M}_\infty(H) = M_3 < 0 \tag{3.5}$$

and

$$\overline{M}_0(H) = M_3 - [(M_1 - M_3)(M_2 - M_3)]^{1/2} \times \frac{\ln[(1 - m\sqrt{2 - m^2})(1 - m^2)^{-1}]^2}{\ln[(3 - m^2 + 2\sqrt{2 - m^2})(1 - m^2)^{-1}]^2} \ , \tag{3.6}$$

where $m^2 = (M_2 - M_3)/(M_1 - M_3) < 1$. The limit $H \to 0$ yields $\lim_{H \to 0} \overline{M}_0(H) = M_1 > 0$. Note that in this limit the bump corresponding to Fig. 1(b) is going over into an antikink (for $\epsilon = +1$) and we have $\xi_2 \to 0, \xi_0 \to -\infty, \xi_1 \to -\infty$. We are thus averaging over a nonsymmetric region (half an antikink). For $\epsilon = -1$ we would have obtained a kink and the limit $-M_1$ for $H \to 0$.

3. Solution (2.5) of Fig. 1(d)

In this case we have either a bump ($\epsilon = +1$), or a well ($\epsilon = -1$). The two possibilities are considered separately. Calculations of the mean magnetization for the bump produce

$$\overline{M}_\infty(H) = M_2 \tag{3.7}$$

and

$$\overline{M}_0(H) = M_2 + [(M_1 - M_2)(M_2 - M_4)]^{1/2} \times \left[\operatorname{arccosh} \left[\frac{2(M_1 + 2M_2)}{M_1 + M_2} \right] \right]^{-1} \times \arccos \left[\frac{M_2 - M_4}{2(M_1 + M_2)} \right] . \tag{3.8}$$

For $H \to 0$ these results reduce to $\overline{M}_\infty(0) = 0$ and $\overline{M}_0(0) = (M_1/3)(\pi/|\operatorname{arccosh} 2|)$. Second, for the well the mean magnetization is found as

$$\overline{M}_\infty(H) = M_2 \ , \tag{3.9a}$$

$$\overline{M}_0(H) = M_2 - [(M_1 - M_2)(M_2 - M_4)]^{1/2} \times \left[\operatorname{arccosh} \left[\frac{2M_1}{M_1 + M_2} \right] \right]^{-1} \times \arccos \left[\frac{M_1 - M_2}{2(M_1 + M_2)} \right] . \tag{3.9b}$$

As $H \to 0$ this reduces to $\overline{M}_\infty(0) = 0$ and $\overline{M}_0(0) = -(M_1/3)(\pi/|\operatorname{arccosh} 2|)$.

B. Periodic solutions

Periodic solutions found in Sec. II include elementary ones (trigonometric) and three different types of Jacobi elliptic functions.

1. Trigonometric solution (2.4) of Fig. 1(c)

The period of this solution is $T = 2\pi[-\Delta(M_1 - M_3)(M_2 - M_3)]^{-1/2}$, and its mean magnetization is

$$\overline{M}(H) = M_3 + [(M_1 - M_3)(M_2 - M_3)]^{1/2} \ . \tag{3.10}$$

Thus, this solution oscillates between M_1 and M_2 satisfying $0<M_2\le M\le M_1$. For a vanishing magnetic field $H\to 0$ we have $M_2\to M_1, M_3\to -M_1$ and the solution tends to a constant $M(\xi)=M_1$ so that $\bar{M}(0)=M_1$.

2. The "snoidal" solution (2.9) of Fig. 1(e)

The real period of this solution is $T=4K(k)/\sqrt{K_0\Delta R}$ where $K(k)\equiv\int_0^{\pi/2}(1-k^2\sin^2\theta)^{-1/2}d\theta$ is the complete elliptic integral of the first kind.[10] The average magnetization over its period is

$$\bar{M}(H)=-\frac{\delta}{\gamma}+\frac{\alpha\delta-\beta\gamma}{\alpha\gamma K(k)}\Pi\left[\frac{\gamma^2}{\alpha^2},k\right], \tag{3.11}$$

where Π is the complete elliptic integral[10] of the third kind. For $H\to 0$ we obtain $\bar{M}(H)\to 0$ as $H\to 0$.

3. The "cnoidal" solution (2.12) of Fig. 1(g)

The real period of this solution is $T=4K(k)/\sqrt{-\Delta AB}$. After lengthy calculations the final result for its mean magnetization is expressed in terms of complete elliptic integrals as

$$\begin{aligned}\bar{M}(H)=&[4(A-B)(M_1-M_2)]^{-1}\{(M_1-M_2)[A(M_1+3M_2)-B(3M_1+M_2)]-(A+B)(A-B)^2\}\\&+\left[\frac{(A+B)(M_1-M_2)}{4K(k)(A-B)}\right]\Pi\left[-\frac{(A-B)^2}{4AB},k\right]\\&+\left[[(A+B)^2-(M_1-M_2)^2]\frac{(A-B)}{4K(k)(A+B)(M_1-M_2)}\right]\Pi\left[\frac{(M_1-M_2)^2}{(A+B)^2},k\right].\end{aligned} \tag{3.12}$$

In the limit $H\to 0$ we have $\lim_{H\to 0}\bar{M}(H)=0$.

4. The "dnoidal" solution (2.11) of Fig. 1(f)

Its period is $T=2K(k)/\sqrt{-\Delta K_0}R$. The final result for $\bar{M}(H)$ is obtained in terms of the normal elliptic integral of the third type[10] as

$$\bar{M}(H)=-\frac{\epsilon\delta R+\beta}{\alpha+\epsilon\gamma R}+\epsilon\frac{\alpha\delta-\beta\gamma}{\alpha^2-\gamma^2R^2}\frac{4R^2}{K(1+R)}\Pi\left[\frac{1+R}{2R}K,\frac{R-1}{R+1}\frac{\epsilon\gamma R+\alpha}{\epsilon\gamma R-\alpha}\right], \tag{3.13}$$

where we have used the definition

$$\Pi(u_1,\alpha^2)\equiv\int_0^{u_1}\frac{du}{1-\alpha^2\mathrm{sn}^2u}.$$

When the field H is switched off, the corresponding solution oscillates between M_2 and M_1 for $\epsilon=+1$ and between $-M_2$ and $-M_1$ for $\epsilon=-1$. The magnetization averaged over one period of the solutions tends to $\epsilon M_1\pi/2K(k)$.

IV. FREE ENERGIES OF INDIVIDUAL SOLUTIONS

The bulk free energy for a given solution is obtained by appropriately integrating the free-energy density f of Eq. (1.1) in which $M(\xi)$ is taken to be a solution of the steady-state LG equation (1.5). In this section we shall run through the solutions of Sec. II and calculate their energies analytically and numerically. It is assumed that the ferromagnetic sample is long and that its cross section is $S_\perp$. The translationally invariant solutions found earlier depend on ξ which is along the length of the sample. Then, the free energy corresponding to a particular translationally invariant solution $M(\xi)$ is

$$F=S_\perp\int_{L_1}^{L_2}d\xi(f_0+\tfrac{1}{2}AM^2+\tfrac{1}{4}BM^4-HM+D\dot{M}^2). \tag{4.1}$$

Using Eq. (2.1) we obtain

$$\frac{F}{S_\perp}=\left[f_0-\frac{BC}{4}\right](L_2-L_1)+\frac{\tilde{F}}{S_\perp}, \tag{4.2}$$

where

$$\begin{aligned}\frac{\tilde{F}}{S_\perp}=&2D\Delta\int_{L_1}^{L_2}(M-M_1)(M-M_2)\\&\times(M-M_3)(M-M_4)d\xi.\end{aligned} \tag{4.3}$$

The first term on the right-hand side of Eq. (4.2) describes the free energy of the constant background. For localized solutions we shall assume that the sample is infinitely long and integrate from $-\infty$ to $+\infty$. For periodic solutions the integration will be performed over their period. Below we calculate the free energies of individual solutions and compare the results with the corresponding cases with no magnetic field ($H\to 0$).

A. Localized solutions

1. Solution (2.2) of Fig. 1(a)

In this case we have

$$\frac{\tilde{F}}{S_\perp}=8\left[\frac{D}{B}\right]\sqrt{-\Delta}H\pi\ . \tag{4.4}$$

Assuming $D<0$ we have $B>0$, $H\geq 0$ $\Delta<0$ and hence $(\tilde{F}/S_\perp)\leq 0$, i.e., its energy is lower than that of the homogeneous background which is understandable in view of the negative sign of D. In the limit of $H\to 0$ this bump solution disappears into the disordered phase ($M=0$) and consequently its free energy vanishes, too: $\tilde{F}/S_\perp\to 0$ as $H\to 0$.

2. Solitary wave (2.3) of Fig. 1(b)

The result here is

$$\frac{\tilde{F}}{S_\perp}=\frac{D(M_2-M_3)^2}{12m^5}[\Delta(M_1-M_3)(M_2-M_3)]^{1/2}\times\left[2m(3m^4-2m^2+3)+3(1-m^2)^2(1+m^2)\ln\left[\frac{1-m}{1+m}\right]\right], \tag{4.5}$$

with $m^2=(M_2-M_3)/(M_1-M_3)$ and $-1<m<1$. Note that the $H\to 0$ limit corresponds to $M_3\to -M_1$, $M_2\to M_1$, and $m\to 1$. This then leads to $\tilde{F}/S_\perp\to 16DM_1^3\sqrt{\Delta}/3$ as $H\to 0$. Comparing this to the kink energy found earlier,[4] $E_{\text{kink}}=4(-A^3D)^{1/2}/3B$, we find that the result above is exactly twice the value of the single kink energy. However, in the previous article[4] the integration was over a semi-infinite region $[0,\infty)$, rather than $(-\infty,+\infty)$ as in the present paper. We therefore conclude that the bump of Eq. (2.3) transforms directly into a kink as $H\to 0$.

3. Solitary wave (2.5) of Fig. 1(d)

The integral required here is elementary and the final result is

$$\frac{\tilde{F}}{S_\perp}=\frac{2D(M_1^2-M_2^2)(M_2-M_4)^2}{3[2M_2+\epsilon(M_1+M_2)]^4}\times[-\Delta(M_1-M_2)(M_2-M_4)]^{1/2}\cdot a^{-5/2}(a+1)^{-2}\times[3(a+1)^2(a-1)\arctan\sqrt{a}+a(3a^2+2a+3)], \tag{4.6}$$

where $a=[2M_2-\epsilon(M_1+M_2)]/[2M_2+\epsilon(M_1+M_2)]$, with $0<a<1$ for $\epsilon=+1$ and $1<a$ for $\epsilon=-1$. The limit $H\to 0$ corresponds to $M_2\to 0$, $M_4\to -M_1$, $a\to 1$ and hence $\tilde{F}/S_\perp\to 4DM_1^3\sqrt{-\Delta}/3$ as $H\to 0$. This agrees perfectly with the value of the free energy obtained for the corresponding bump solution in the previous paper.[4]

B. Periodic solutions

1. Trigonometric solution (2.4) of Fig. 1(c)

The final result in this case is

$$\frac{\tilde{F}}{S_\perp}=\frac{D\pi}{2}(M_1-M_2)^2(M_1+M_2)\sqrt{-\Delta}\ . \tag{4.7}$$

In the limit $H\to 0$ we have $M_1\to M_2$ and the solution goes over into a constant one ($M=M_1$). Consequently, the free energy contribution in (4.7) vanishes and only the background term in (4.2) survives.

2. The snoidal wave solution (2.9) of Fig. 1(e)

The free energy can be expressed as

$$\frac{\tilde{F}}{S_\perp}=\frac{2D\Delta}{\sqrt{\Delta K_0}R}(M_1\gamma+\delta)(M_2\gamma+\delta)(M_3\gamma+\delta)(M_4\gamma+\delta)\times\int_0^{4K}\frac{[R^2-\mathrm{sn}^2(u,k)][1-\mathrm{sn}^2(u,k)]}{[\alpha-\gamma\,\mathrm{sn}(u,k)]^4}du\ . \tag{4.8}$$

The integral can be evaluated in terms of complete elliptic integrals, but we shall not present this here, since the result is not very illuminating. In the limit $H\to 0$ we have $M_3=-M_2$, $M_4=-M_1$, $k=1/R=M_2/M_1$, $\beta=0$, $\gamma=0$, $\delta/\alpha=M_2$, $K_0=M_2^2$ so that $\tilde{F}/S_\perp$ reduces to precisely the integral evaluated in our earlier paper[4]

$$\left.\frac{\tilde{F}}{S_\perp}\right|_{H=0}=2D\sqrt{\Delta}M_1M_2^2\times\int_0^{4K}[1-k^2\mathrm{sn}^2(u,k)][1-\mathrm{sn}^2(u,k)]du\ . \tag{4.9}$$

3. The dnoidal wave solution (2.11) of Fig. 1(f)

The expression for the free energy integrated over one period can be expressed as

$$\frac{\tilde{F}}{S_\perp}=2D\sqrt{-\Delta}R^3(\alpha\delta-\beta\gamma)\times[(M_1\gamma+\delta)(M_2\gamma+\delta)(M_3\gamma+\delta)(M_4\gamma+\delta)]^{1/2}\times\int_{-K}^{K}\frac{[1-\mathrm{dn}^2(u,k)][\mathrm{dn}^2(u,k)-k'^2]}{[\alpha-\gamma R\,\mathrm{dn}(u,k)]^4}du\ . \tag{4.10}$$

Again, although this is doable we shall not express this integral in terms of elliptic functions since the result is very complicated in form. In the limit $H\to 0$, we have complete agreement with our previous result,[4] namely

$$\left.\frac{\tilde{F}}{S_\perp}\right|_{H=0}=2D\sqrt{-\Delta}M_1^3\int_{-K}^{K}[(1-\mathrm{dn}^2(u,k)]\times[\mathrm{dn}^2(u,k)-k'^2]du\ . \tag{4.11}$$

4. The cnoidal wave solution (2.12) of Fig. 1(g)

The contribution of the cnoidal waves to the free energy over one period is

$$\frac{\tilde{F}}{S_\perp}=2D\sqrt{-\Delta}(AB)^{3/2}(M_1-M_2)^2\frac{(A+B)^2-(M_1-M_2)^2}{(A+B)^4(1-k^2)}\times\int_0^{4K}\frac{[(1-\mathrm{cn}^2(u,k)][k'^2+k^2\mathrm{cn}^2(u,k)]}{\{1+[(A-B)/(A+B)]\mathrm{cn}(u,k)\}^4}du\ . \tag{4.12}$$

In the $H\to 0$ limit (4.12) reduces to the case integrated explicitly in our previous article[4]

$$\left.\frac{F}{S_\perp}\right|_{H=0}=2D\sqrt{-\Delta}M_1^2\sqrt{M_1^2+q^2}\times\int_0^{4K}[1-\mathrm{cn}^2(u,k)][k'^2+k^2\mathrm{cn}^2(u,k)]du\ . \tag{4.13}$$

V. DISCUSSION AND CONCLUSIONS

This paper has been concerned with a Landau-Ginzburg model of a uniaxial ferromagnet with inhomogeneities in the presence of an external magnetic field. Having presented the results of symmetry reduction analysis for the steady-state equation of state we have completely analyzed the most important case, translationally invariant solutions. This included the analytical form of all the magnetization profiles $M(\xi)$, the mean magnetization values and free energies required for their formation. A summary of all these results is given in Table I to assist the reader. It can be concluded that localized solutions which may only be in the form of bumps for $H\neq 0$ possess a finite energy and when defined over a finite domain have a nonzero magnetization above the mean field background. Periodic solutions in the form of several types of elliptic waves describe classical spin waves which may be of ferromagnetic or antiferromagnetic kind. all of these waves have finite energy densities and their mean magnetizations are expressed in terms of elliptic integrals.

We have also found, very much in analogy with the earlier calculations for the case with no field, that for $D>0$ (ferromagnetic nearest neighbors) the spectrum of the free-energy functional is bounded both from above and below while for $D<0$ only from above. The latter case corresponds to the antiferromagnetic nearest-neighbor interactions and it leads, in continuum approximation, to a structural instability of its solutions with a tendency to acquire uncontrollably high frequencies and amplitudes. It can thus be called a modulational instability. This problem, however, can be solved by imposing a lower bound on the wavelength of solutions due to the existence of lattice periodicity in the spin system.

Finally, we wish to comment on a particular application to which our analysis may find use, namely to the explanation of details of the shape of the so-called Arrott plot. Many years ago, Arrott[12] introduced a convenient way of analyzing experimental data concerning magnetization processes of ferromagnetic materials. He proposed to plot H/M versus M^2 rather than $M=M(H)$ in order to obtain a predominantly linear dependence and

TABLE I. Summary of the results obtained in the paper.

Solution	Type	Part of Fig. 1	Mean magnetization	Energy	Sketch
(2.2)	Algebraic bump or well	(a)	(3.3) (3.4)	(4.4)	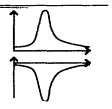
(2.3)	Hyperbolic bump or well	(b)	(3.5) (3.6)	(4.5)	
(2.4)	Trigonometric wave	(c)	(3.10)	(4.7)	
(2.5)	Hyperbolic bump or well	(d)	(3.7) (3.8)	(4.6)	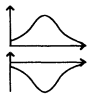
(2.9)	Elliptic waves (sn)	(e)	(3.11)	(4.8)	
(2.11)	Elliptic waves (dn)	(f)	(3.13)	(4.10)	
(2.12)	Elliptic waves (cn)	(g)	(3.12)	(4.12)	
(2.13)	Constant	(c), (h) isolated circles			

avoid multivaluedness. Indeed, the thus obtained Arrott plot is usually linear. However, it was observed early on[9] that close to the origin of this coordinate system the curvature of the plot becomes quite pronounced and it develops a downward trend. One of the most recent sets of experimental data to conform with this characterization is concerned with Fe_3O_4 submicronic particles.[13] Several possible explanations of the effect have been put forward including random anisotropy[14] but so far no consensus on the answer to this question has emerged.

Based on the results of our analysis concerning the forms of $M(\xi)$ which minimize the free-energy functional (and thus are most likely to play an important physical role) we wish to investigate the possibility of a particular effect causing the curvature of the Arrott plot. First, the homogeneous phases, $M=\text{const}$, satisfy the equation of state (1.5), which upon rearranging becomes

$$y \equiv \frac{H}{M} = A + Bx, \quad \text{where } x \equiv M^2 , \tag{5.1}$$

assuming that $M \neq 0$. This is precisely the straight line behavior in the "idealized" Arrott plot. We have illustrated this graphically in Fig. 2(a). Of course, if the mean phase considered here is to be stable, it must be in addition required that

$$\frac{\partial^2 F_0}{\partial M^2} = A + BM^2 = A + Bx \geq 0 , \tag{5.2a}$$

where F_0 is the free energy of the mean field, i.e.,

$$F_0 = \tfrac{1}{2} AM^2 + \tfrac{1}{4} BM^4 - HM . \tag{5.2b}$$

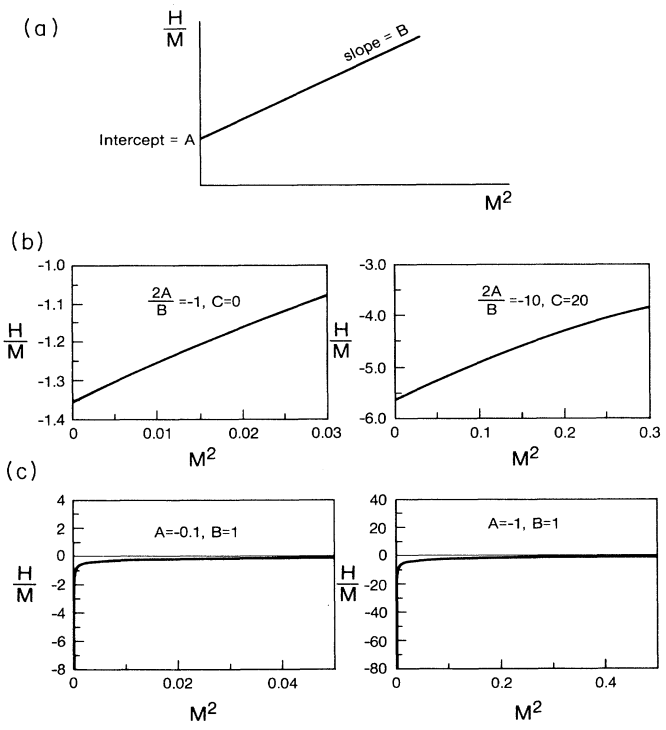

FIG. 2. Arrott plots obtained for particular types of solutions: (a) constant, (b) snoidal waves, (c) bump solitons.

Thus, mean equilibrium phases will *not* provide a satisfactory explanation of the said curvature. Next, consider periodic solutions found earlier in the form of elliptic functions. Their mean magnetization can usually be well approximated by the midvalue between the two turning points M_1, M_2 (especially for the low-energy ones which should contribute the most). This then gives

$$\overline{M} \cong \frac{M_1 + M_2}{2} \cong M_0 , \tag{5.3}$$

where M_0 is the extremal value of the plot $(dM/d\xi)^2$ as a function of M, which lies between M_1 and M_2. Since M_0 is an extremum of $F(M)$, it satisfies Eq. (5.1) yielding

$$\frac{H}{M_0} = A + BM_0^2 . \tag{5.4}$$

Once again, we must conclude that these solutions will very closely obey the standard Arrott plot form. In Fig. 2(b) we have demonstrated this for snoidal waves with various values of the Jacobi modulus k. A small curvature can be seen which becomes more and more pronounced as $k \to 1$, i.e., as they tend to the bump soliton [Fig. 2(c)].

Finally, consider the localized solutions in the form of bumps. We have seen in Sec. II that

$$\overline{M} = M_- + \Delta\overline{M} , \tag{5.5}$$

where M_- is the double root of $(dM/d\xi)^2$ versus M which corresponds to the higher-energy (metastable) phase when H is switched on. The small correction $\Delta\overline{M}$ is in the direction of the stable phase M_+ which is oriented along the field H. Since M_- is a double root, it too satisfies Eq. (5.4) or

$$AM_- + BM_-^3 = H . \tag{5.6}$$

Substituting (5.5) into (5.6) and keeping only linear terms in $\Delta\overline{M}$ yields

$$A\overline{M} + B\overline{M}^3 - (A + 3B\overline{M}^2)\Delta\overline{M} = H , \tag{5.7}$$

but the coefficient multiplying $\Delta\overline{M}$ is

$$A + 3B\overline{M}^2 \cong \left[\frac{\partial^2 F}{\partial M^2}\right]\Bigg|_{M=M_-} \geq 0 , \tag{5.8}$$

i.e., it represents the positive curvature of the free-energy plot $F_0(M)$ close to its extremum M_- and hence, it is approximately independent of the field for small values of H. As $H \to H_c$, however, $A + 3B\overline{M}^2 \to 0$ [since we approach an inflection point of $F_0(M)$] and the extra term in Eq. (5.7) disappears. In terms of the Arrott plot we have

$$A + Bx - \frac{\tilde{\Delta}}{\sqrt{x}} = y , \tag{5.9}$$

where $\tilde{\Delta} = (A + 3B\overline{M}^2)\Delta\overline{M} \geq 0$ and $x \neq 0$. This is graphically illustrated in Fig. 2(c). We may therefore conclude the following.

(i) Bumps (representing nucleation centers of the metastable magnetic phase) produce a curvature of the Arrott

plot close to the origin.

(ii) The curvature produced is in the right direction since $\tilde{\Delta} \geq 0$, based on thermodynamic stability.

(iii) The curvature should be sensitive to temperature, i.e., diminish as $T \rightarrow T_c$.

(iv) Since $\Delta \overline{M}$ is in fact proportional to the density of bumps (their number per unit length) and the latter should increase with the number of defects, we expect the curvature to be more pronounced in polycrystalline samples than in monocrystals (exactly as shown by experiment).

(v) Since $A + 3B\overline{M}^2 \rightarrow 0$ as $H \rightarrow H_c$, starting from $H = H_c$ the curvature should disappear completely. It so happens that at $H = H_c$ bumps are no longer allowed either.

Magnetic inhomogeneities were indeed previously linked with the curvature of the Arrott plot[3,15,16] but a direct link has never before been demonstrated. In fact, comparing the results of our analysis[4] for $H = 0$ with those for $H \neq 0$, we note that the effect of applying an external magnetic field is to disallow kink solutions (domain walls) as results of minimization of the free energy and replace them by bump solutions (nucleation centers). Since the Arrott plot is basically a special way of drawing the dc susceptibility of a magnet (i.e., χ^{-1} versus M^2), we conclude that its curvature in the range $0 \leq H \leq H_c$ manifests the dynamics of localized magnetization profiles in the form of nucleation centers of the metastable phase.

It should be added in closing that for large values of x $(= M^2)$ the presence of a sixth power term in the free-energy expansion could manifest itself in another type of nonlinearity in the Arrott plot.[17] This would also lead to a very interesting possibility of double hysteries loops experimentally observed in ferroelectrics.[18]

A question that has been investigated recently[19] is the stability of exact solutions of the quartic Landau-Ginzburg equation without an external field $(H = 0)$. Most of the solutions turn out to be unstable with respect to certain types of time-dependent perturbation. The physical implications of this remain to be investigated. In any case nonstable solutions may represent transient phenomena that may be quite important.

ACKNOWLEDGMENTS

This research project has been supported by grants from the Natural Sciences and Engineering Research Council of Canada. P.W. also acknowledges partial support by the "Fonds FCAR du Gouvernement du Québec."

[1] M. Luban, in *Phase Transitions and Critical Phenomena,* edited by C. Domb and M. S. Green (Academic, London, 1976), Vol. 5A.

[2] L. D. Landau and E. M. Lifshitz, *Statistical Physics* (Pergamon, London, 1980).

[3] W. I. Khan, J. Phys. C **19**, 2969 (1986).

[4] P. Winternitz, A. M. Grundland, and J. A. Tuszyński, J. Phys. C **21**, 4931 (1988).

[5] A. T. Aldred, J. Magn. Magn. Mater. **10**, 42 (1979).

[6] D. Wagner and E. P. Wohlfarth, J. Magn. Magn. Mater. **15-18**, 1345 (1980).

[7] P. W. Anderson, Basic Notions of Condensed Matter Physics (Benjamin/Cummings, Menlo Park, CA, 1984).

[8] P. Olver, *Applications of the Lie Groups to Differential Equations* (Springer-Verlag, New York, 1986).

[9] W. Sucksmith and J. E. Thompson, Proc. R. Soc. London **225**, 362 (1954).

[10] P. F. Byrd and M. D. Friedman, *Handbook of Elliptic Intergrals for Engineers and Scientists* (Springer, Berlin, 1971).

[11] M. Shimizu, J. Phys. (Paris) **43**, 155 (1982).

[12] A. S. Arrott, Phys. Rev. **108**, 1394 (1957).

[13] S. Arajs, N. Amin, and E. E. Anderson, Phys. Rev. B **35**, 4810 (1987).

[14] A. Aharony and E. Pytte, Phys. Rev. Lett. **45**, 1583 (1980).

[15] F. P. Wohlfarth (unpublished).

[16] F. Acker, Z. Fisk, J. L. Smith, and C. Y. Huang, J. Magn. Magn. Mater. **22**, 250 (1981).

[17] W. I. Khan and D. Melville, J. Magn. Magn. Mater. **36**, 256 (1983).

[18] J. A. Tuszyński, B. Mroz, H. Kiefte, and M. J. Clouter, Ferroelectrics **77**, 111 (1988).

[19] A. M. Grundland, E. Infeld, G. Rowlands, and P. Winternitz, J. Phys. Condens. Matter **2**, 7143 (1990).